# Supplementary Material: Drivers of decadal hiatus periods in the 20th and 21st Centuries

Nicola Maher,[1,2] Alexander Sen Gupta,[1,2] Matthew H. England,[1,2]

Corresponding author: N. Maher, Climate Change Research Centre, Level 4, Mathews Building, University of New South Wales, Sydney, NSW, Australia, 2052. (n.maher@unsw.edu.au)

[1]Climate Change Research Centre,
University of New South Wales, NSW,
Australia.

[2]ARC Centre of Excellence for Climate
System Science, University of New South
Wales, NSW, Australia.

## 1. Methods

Accelerated decade thresholds are defined separately for each scenario using the mid-point of the mean and maximum decadal trends. These values are set as 0.48 $^o$C/decade for both the historical (mean = 0.067 $^o$C/decade and max = 0.90 $^o$C/decade) and RCP4.5 (mean = 0.18 $^o$C/decade and max = 0.78 $^o$C/decade) scenarios and 0.85 $^o$C/decade for the RCP8.5 (mean = 0.42 $^o$C/decade and max = 1.36 $^o$C/decade) scenario.

Interdecadal Pacific Oscillation (IPO) time-series are calculated for only 27 of the 31 CMIP5 models due to data availability (see Supplementary Table 1). In order to maintain a consistent IPO definition across all simulations of a given model, an EOF analysis is undertaken using 13-year filtered sea surface temperature (SST) anomalies from each model's control simulations (subject to fixed greenhouse gas concentrations, set at pre-industrial levels) for the Pacific region (40$^o$S-60$^o$N and 100$^o$E-70$^o$W) [**????**]. The first principal component is regressed against the filtered time-series at each point to compute the IPO spatial pattern (Supplementary Figure 3). The IPO spatial patterns are regressed against filtered SST from the forced scenarios, to compute the respective IPO time-series. Due to the filter used we cannot use the beginning or end of the time-series. The control simulations are generally run between 250 and 1000 years after model spin-up and only change as a result of internal variability (although a small amount of spurious climate drift may also be present [**?**]).

The El Niño Southern Oscillation (ENSO) index is computed to investigate the La Niña-like pattern found in the SAT trend composites around volcanic eruptions. ENSO indices are computed using detrended and de-seasonalised monthly data for the historical scenario,

using the same 27 models used to compute the IPO index. The ENSO time-series is taken to be the first principal component from an EOF analysis over the region $30^o$S-$30^o$N and $100^o$E-$70^o$W. The ENSO index is composited over the four major volcanic eruptions to examine the typical evolution of ENSO phase before and after a major volcanic eruption, effectively using each eruption as an ensemble member. A multi-model mean composite is then computed. To examine whether the multi-model mean ENSO index evolution is statistically robust, four randomly selected decades from the historical simulation for a given model are averaged to compare against the four volcanic periods, and then averaged between models. This process is repeated 1000 times to find the spread of results and the 5th and 95th percentiles are computed. If the multi-model mean index sits outside these percentiles, then the index value is considered to be significantly different from a random process.

The main text outlines two artificial volcanic eruptions, which are constructed to examine the influence a volcano may have on surface air temperature (SAT) in the future. To modify the RCP4.5 and RCP8.5 SAT time-series to account for the volcanic eruptions a multiple linear regression is performed over the historical period to determine the response of SAT to the different forcing: volcanic, solar, anthropogenic (greenhouse gases and aerosols) and ENSO.

$$SAT = a * solar + b * volcanic + c * anthropogenic + d * ENSO \quad (1)$$

Where a,b,c and d are coefficients determined by the regression analysis. To generate the modified future time-series, the synthetic volcanic radiative forcing are scaled by the

Table 1: CMIP5 models used in the analyses completed in this paper. Models shown in this table are used in the SAT analysis (all three scenarios: historical, RCP4.5 and RCP8.5). The subset of models used to complete the IPO and ENSO analyses is shown, here 4 models were not available for use. We also outline the 13 models that have IPO patterns that correlate over 0.7 with the IPO pattern calculated from observations.

| Institute | Model | Used in: IPO and ENSO analyses | IPO >0.7 correlation with HadISST |
|---|---|---|---|
| CSIRO-BOM | ACCESS1.0 | Y | **Y** |
| CSIRO-BOM | ACCESS1.3 | Y | **Y** |
| BCC | BCC-CSM1.1 | Y | N |
| CCCMA | CanESM2 | Y | **Y** |
| NCAR | CCSM4 | Y | N |
| NSF-DOE-NCAR | CESM1(BGC) | Y | N |
| NSF-DOE-NCAR | CESM1(CAM5) | Y | **Y** |
| CMCC | CMCC-CM | Y | **Y** |
| CMCC | CMCC-CMS | Y | **Y** |
| CNRM-CERFACS | CNRM-CM5 | Y | N |
| CSIRO-QCCCE | CSIRO-Mk3.6.0 | Y | **Y** |
| LASG-CESS | FGOALS-g2 | N | N |
| LASG-CESS | FOGALS-s2 | N | N |
| NOAA GFDL | GFDL-CM3 | N | N |
| NOAA GFDL | GFDL-ESM2G | Y | N |
| NOAA GFDL | GFDL-ESM2M | Y | N |
| NASA GISS | GISS-E2-H | Y | N |
| NASA GISS | GISS-E2 -R | Y | N |
| NIMR/KMA | HadGEM2-AO | N | N |
| MOHC | HadGEM2-CC | Y | N |
| MOHC | HadGEM2 -ES | Y | **Y** |
| INM | INM-CM4 | Y | N |
| IPSL | IPSL-CM5A-LR | Y | **Y** |
| IPSL | IPSL-CM5A-MR | Y | **Y** |
| IPSL | IPSL-CM5B-LR | Y | N |
| MIROC | MIROC-ESM | Y | N |
| MIROC | MIROC5 | Y | **Y** |
| MPI-M | MPI-ESM-LR | Y | **Y** |
| MRI | MRI-CGCM3 | Y | **Y** |
| NCC | NorESM1-M | Y | N |
| NCC | NorESM1-ME | Y | N |

associated volcanic regression coefficient, and the resulting temperature anomaly is added to the RCP4.5 and RCP8.5 SAT time-series.

## References


Arblaster, J., G. Meehl, and A. Moore (2002), Interdecadal modulation of Australian rainfall, *Climate Dynamics*, *18*, 519–531.

Folland, C. K., D. E. Parker, and A. Colman (1999), Large scale modes of ocean surface temperature since the late nineteenth century., in *Beyond El Nino: decade 1 and interdecade 1 climate variability*, edited by A. Navarra, pp. 73–102, Springer, Berlin Heidelberg New York.

Meehl, G., A. Hu, J. Arblaster, J. Fasullo, and K. E. Trenberth (2013), Externally forced and internally generated decadal climate variability associated with the Interdecadal Pacific Oscillation, *Journal of Climate*, *26*, 7298–7310.

Power, S., T. Casey, C. Folland, A. Colman, and V. Mehta (1999), Inter-decadal modulation of the impact of ENSO on Australia, *Climate Dynamics*, *15*, 319–324.

Rayner, N. A., D. E. Parker, E. B. Horton, C. K. Folland, L. V. Alexander, D. P. Rowell, E. C. Kent, and A. Kaplan (2003), Global analyses of sea surface temperature, sea ice, and night marine air temperature since the late nineteenth century, *Journal of Geophysical Research*, *108*(D14), doi:10.1029/2002JD002670.

Sen Gupta, A., N. C. Jourdain, J. N. Brown, and D. Monselesan (2013), Climate Drift in the CMIP5 Models, *Journal of Climate*, *26*(21), 8597–8615.

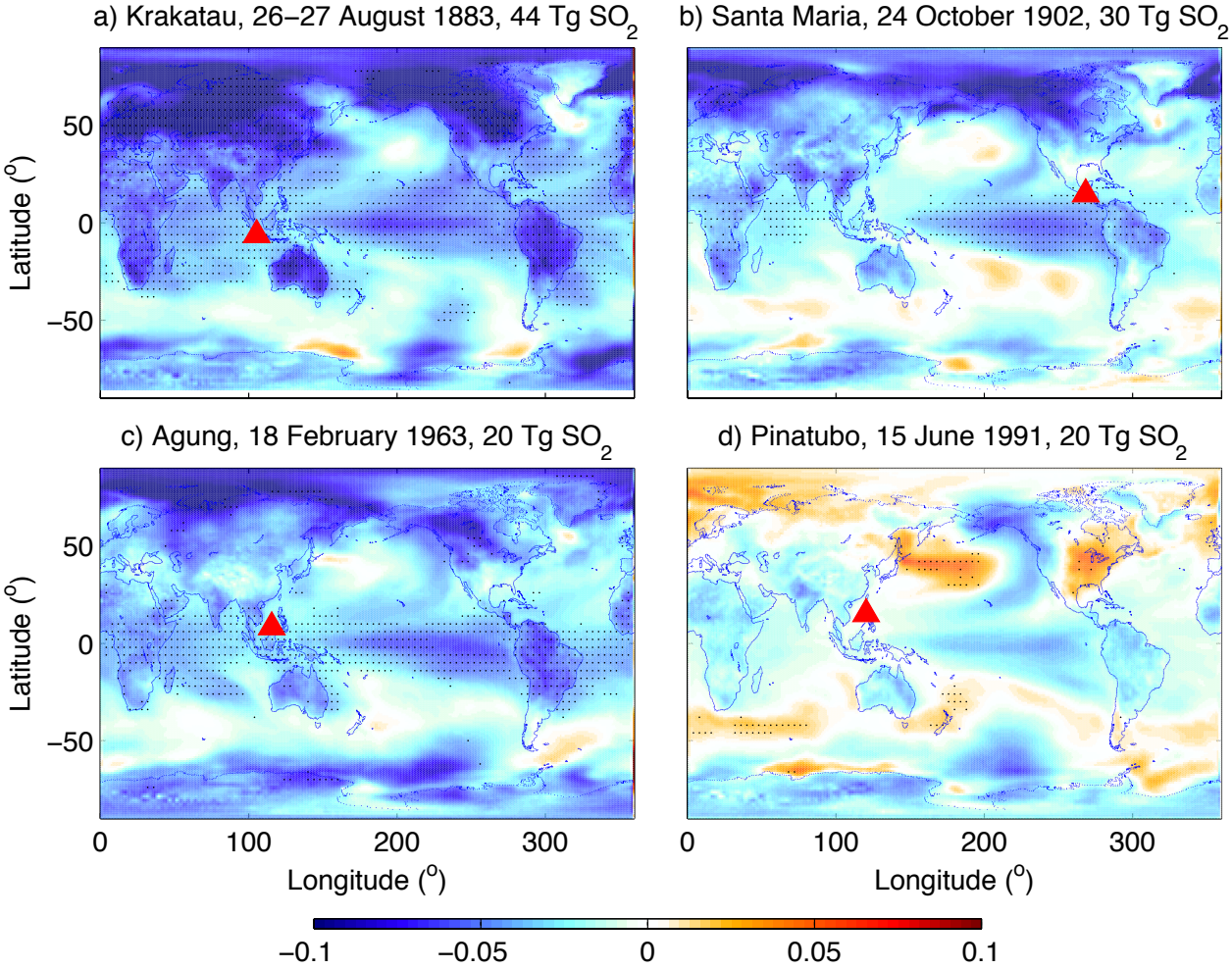


Figure 1: The composite spatial pattern of surface air temperature trends ($^o$C/year) during hiatus decades (10 year trend less than zero) for the 4 largest historical volcanic eruptions: a) Krakatau 1883 (number of models with hiatus = 31), b) Santa Maria 1902 (number of models with hiatus = 29), c) Agung 1963 (number of models with hiatus = 30) and d) Pinatubo 1991 (number of models with hiatus = 22). The location of the eruption is represented by a red triangle. Stippling is shown to when 80% of the models agree on the sign of the trend.

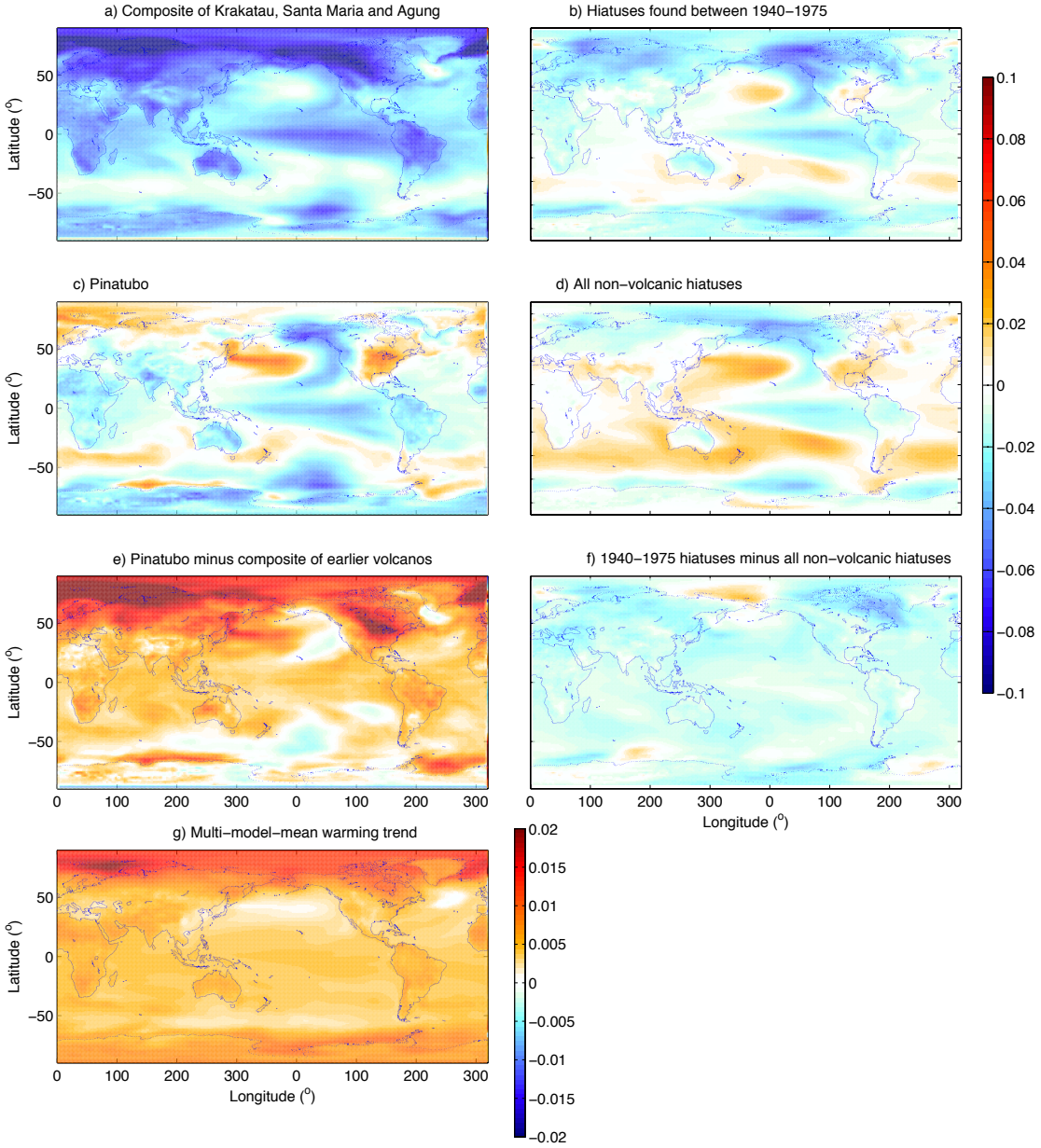


Figure 2: a) The mean of the composite spatial trend patterns of SAT ($^o$C/year) for the three earlier volcanic eruptions (Krakatau - 1883, Santa Maria - 1902 and Agung - 1963). b) The composite spatial SAT trend pattern ($^o$C/year) for all hiatus periods found between 1940 and 1975. c) The composite spatial SAT trend pattern ($^o$C/year) for the Pinatubo (1991) eruption. d) The composite spatial SAT trend pattern ($^o$C/year) for all non-volcanic hiatus decades found in the historical period. e) The difference between the Pinatubo eruption and the three earlier eruptions ($^o$C/year). f) The difference between hiatus decades found in the period 1940-1975 and those found for the entire historical record ($^o$C/year). g) Multi model mean warming trend calculated over the period 1915-1991 ($^o$C/year).

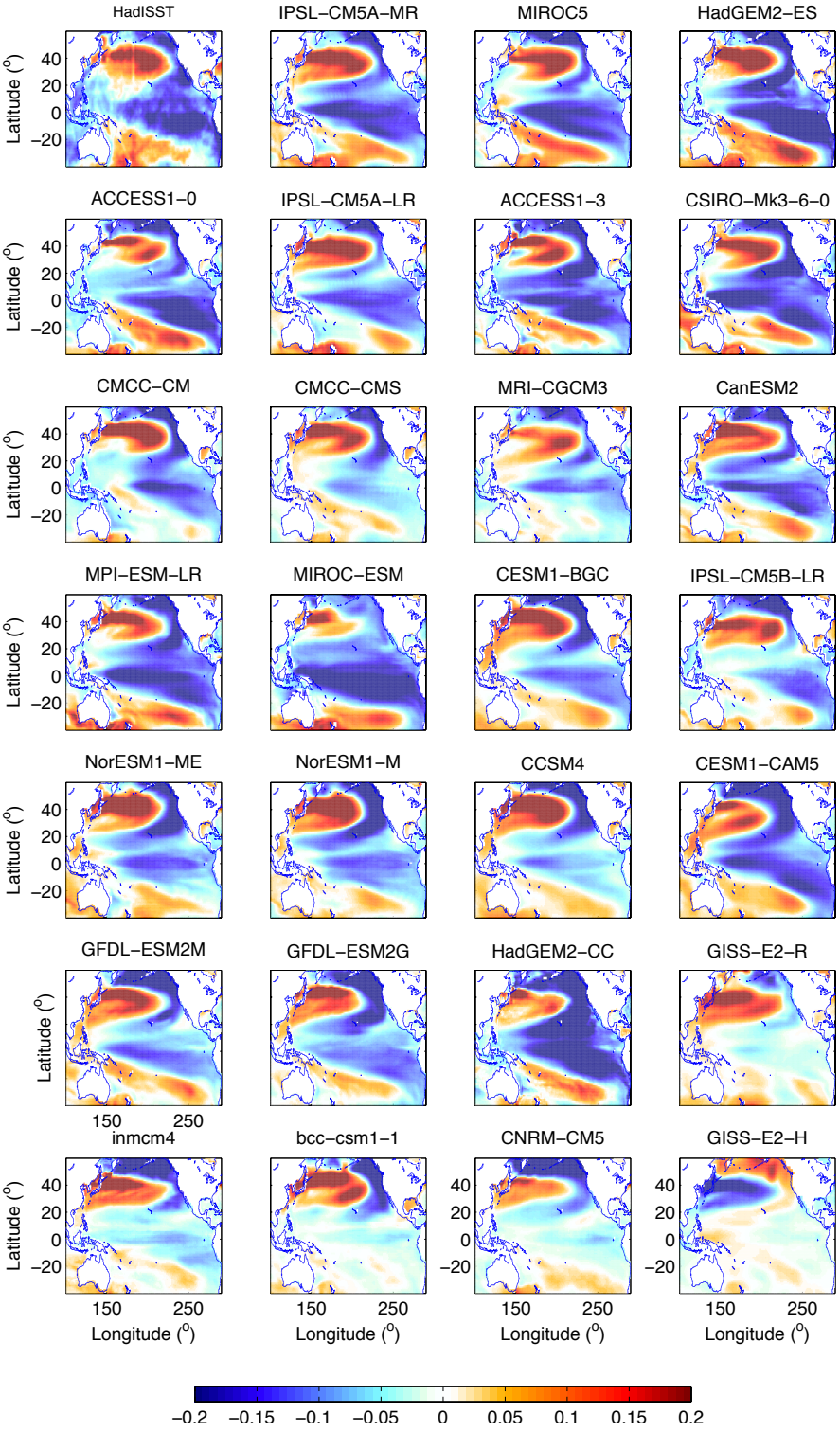


Figure 3: The first panel shows the negative IPO pattern calculated as the first EOF of 13 year filtered and detrended data (HadISST [**?**]) and regressed back onto the filtered data. The following panels are the negative IPO calculated for 27 CMIP5 models using the pre-industrial control run. Models are ordered from most to least pattern correlated with the observed pattern in the Pacific.

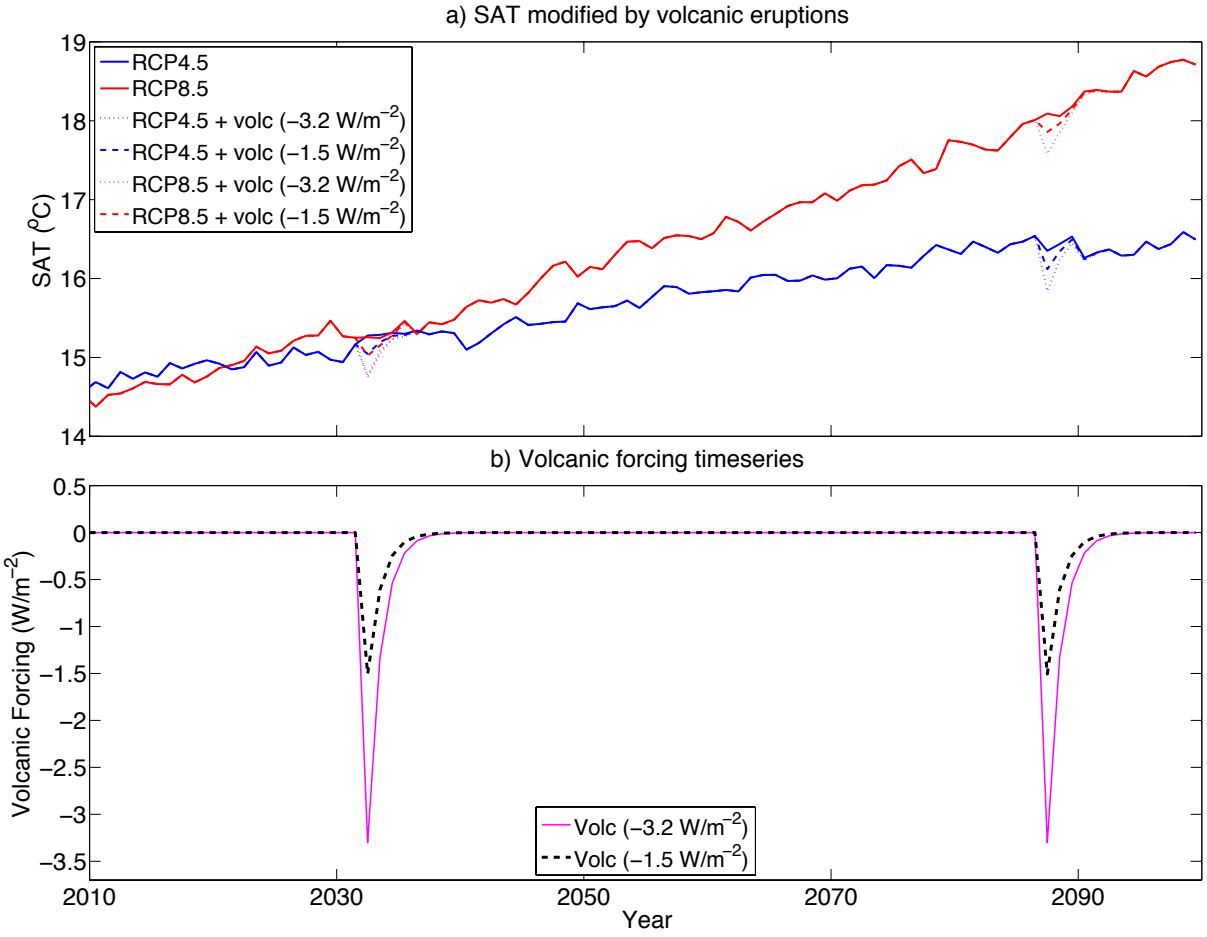


Figure 4: a) SAT for the RCP4.5 (blue) and RCP8.5 (red) future scenarios in the ACCESS1-0 model. The effect of two different sized volcanic eruptions, Santa Maria size (dashed lines) and Krakatau sized (dotted lines) if they occurred in 2032 and 2087 are shown. b) Artificial annual radiative forcing from two volcanic eruptions in 2032 and 2087, Santa Maria (dashed black) and Krakatau (purple) sized. See methods section for details on the construction of the artificial time series and modification of SAT.